ELSEVIER

Journal of Nuclear Materials 303 (2002) 73–81

journal of nuclear materials

www.elsevier.com/locate/jnucmat

Corrosion resistance of structural materials to Ga_2O at 1000 °C

Todd O. Sullivan [a], Nathan A. Byman [a], Frédéric Landry [a], David G. Kolman [b], Eric M. Taleff [a,*]

[a] *Department of Mechanical Engineering, Materials Science and Engineering Program, University of Texas at Austin, Austin, TX 78712-1063, USA*

[b] *Los Alamos National Laboratory, Nuclear Materials Technology Division, Los Alamos, NM 87545, USA*

Received 3 July 2001; accepted 17 January 2002

Abstract

The thermally-induced gallium removal (TIGR) process is capable of removing gallium from oxide powders through the sublimation of Ga_2O at elevated temperatures in a reducing atmosphere. Heat-resistant structural materials typically used in the construction of furnaces and reaction chambers may be susceptible to embrittlement and corrosion in the gallium-rich environment of the TIGR process. The susceptibilities of several heat-resistant structural materials to corrosion in Ga_2O-rich atmospheres are experimentally evaluated. Tungsten and SiC are found to be highly resistant to corrosive attack by Ga_2O at elevated temperatures. Superalloys containing chromium and cobalt as well as a tungsten alloy containing nickel and copper are found susceptible to corrosive attack by gallium.

1. Introduction

The thermally-induced gallium removal (TIGR) process was developed at the Los Alamos National Laboratory for application to the production of mixed-oxide fuel (MOX) for light water reactors. The Ga content of MOX must be very low to prevent potential embrittlement of the zirconium alloy (Zircaloy) cladding materials used for reactor fuel rods [1,2]. TIGR offers a practical method by which Ga can be removed from the oxide powders used to produce MOX while creating significantly less waste material than competing processes. TIGR takes advantage of the sublimation of Ga_2O from Ga_2O_3, which readily occurs in a reducing atmosphere at temperatures above 500 °C [3,4]. Laboratory experiments have demonstrated that Ga concentrations in MOX can be reduced to 1 ppm by using the TIGR process [5]. In these experiments an atmosphere of Ar–6%H_2 was used at a temperature of 1200 °C. Vapor-phase Ga_2O was removed by gas flow past the oxide powders. For high rates of Ga removal by the TIGR process, temperatures in the range of 1000–1200 °C are desirable. Unfortunately, many of the heat-resistant structural materials typically used for the construction of furnaces and reaction chambers at these temperatures are potentially susceptible to embrittlement and corrosion in a Ga-rich environment. Although Ga is present as Ga_2O_3 and Ga_2O for the TIGR process, the deposition of Ga metal on furnace parts is possible [4].

Many metallic materials are susceptible to corrosive attack by Ga through a variety of corrosion processes and reactions. These include uniform corrosion, liquid metal embrittlement, and solid metal induced embrittlement [2,6]. Unfortunately, data on the susceptibility of structural materials to corrosion by Ga at elevated temperatures are scarce [7–9]. Among metals, tungsten and tantalum exhibit the greatest resistance to Ga attack, while solid platinum and platinum group elements are attacked at elevated temperatures [7]. Little information is available on the resistance of ceramics to Ga

* Corresponding author. Address: Department of Mechanical Engineering, University of Texas at Austin, 160 East Dean Keeton Street, Austin, TX 78705, USA. Tel.: +1-512 471 5378; fax: +1-512 471 7681.

E-mail address: taleff@mail.utexas.edu (E.M. Taleff).

0022-3115/02/$ - see front matter
PII: S0022-3115(02)00796-1

attack, although Ga is known to dissolve readily in Al_2O_3, creating solid solution $GaAlO_3$ [11]. Several heat-resistant structural materials were chosen for evaluation of their susceptibilities to corrosion in a Ga-rich environment similar to that seen in the TIGR process.

Five commercially-available materials were selected for study: two superalloys, a refractory metal alloy, a pure refractory metal, and a structural ceramic. The two superalloys include one Ni-based material, Alloy 625, and one Co-based material, Stellite 6. The refractory metal, high-purity W, and refractory alloy, W–Cu–Ni, were included because of their high melting temperatures and the known resistance of W to Ga attack at lower temperatures. High-purity W was in the form of foils, while other metals were in bulk form. The structural ceramic SiC was included in this study because of its strength at elevated temperatures, expected stability in a Ga_2O-rich reducing atmosphere, and ability to be applied as a coating. The composition of each material is shown in Table 1 as wt%.

2. Experimental procedures

A sample of each material in its as-received condition was prepared for microstructural observations using standard metallographic preparation techniques. Polished and etched surfaces of each material were observed under optical and scanning-electron microscopes. Samples of the metallic alloys were etched for microstructural examination. Stellite 6 was etched with a mixture of HCl and H_2O_2 in water, Alloy 625 was etched with Marble's reagent ($CuSO_4$ and HCl in water), and the W alloy was etched with glyceria (HCl and HNO_3 in glycerol). Samples of each material were prepared for exposure experiments and exposed to a controlled, Ga-rich environment in vacuum-sealed ampoules of fused silica held in a furnace at 1000 °C for various times. Samples of each material were cut to size with a low-speed diamond saw. Sample masses varied from 2 to 10 g, except for the SiC and pure W samples, which had masses from 0.22 to 0.41 g. One surface of each metal alloy sample was prepared for exposure experiments by grinding and polishing procedures typical of metallographic preparation. The chosen surface was first ground with progressively finer SiC papers, followed by polishing with progressively finer diamond pastes to a final polish with a 1 μm diamond compound. One corner of each sample was ground at an angle to allow easy identification of the polished surface after exposure experiments. The SiC sample surfaces were prepared by grinding only with diamond abrasives. Each sample was thoroughly cleaned using an ultrasonic cleaner, rinsed in deionized water, dried, and weighed on a precision balance prior to inclusion in an ampoule.

Two types of ampoules were used, each containing only one sample per ampoule. The first ampoule type, shown in Fig. 1(a), contained one sample, Ga_2O_3 powder, and a pipette with one end open containing liquid Ga; the liquid Ga in the pipette was open to the atmosphere in the ampoule but separated from the Ga_2O_3 powder and sample. The second ampoule type, shown in Fig. 1(b), contained one sample and a permeable plug of fused silica wool separating the sample from Ga_2O_3 powder and a small amount of liquid Ga. The presence of liquid Ga stabilizes the partial pressure of O_2 during the experiments, according to the following reactions:

$$Ga_2O_3(s) \rightarrow Ga_2O(g) + O_2(g), \quad (1)$$

$$4\,Ga(l) + 3\,O_2(g) \rightarrow 2\,Ga_2O_3(s), \quad (2)$$

$$4\,Ga(l) + O_2(g) \rightarrow 2\,Ga_2O(g). \quad (3)$$

The Ga_2O_3 powder and liquid Ga used each have a minimum purity of 99.99%. Each ampoule was evacuated under high vacuum for an extended period, with moderate heating early in the process to release water vapor from the Ga_2O_3 powder, which is hygroscopic. A minimum vacuum of 10^{-4} Torr was achieved in each ampoule. Following evacuation, each fused silica ampoule was sealed.

Exposure experiments were conducted using sealed ampoules individually heated in a furnace for from 2 to 20 h. A resistance tube furnace was used to heat each ampoule, and temperature was measured with a type K thermocouple placed next to the ampoule. The furnace was preheated to 1000 °C prior to insertion of the ampoule. The choice for exposure times of up to 20 h was established based on several preliminary experiments to

Table 1
Nominal compositions of the materials tested are given as wt%

Material	C	Al	Si	P	S	Ti	Cr	Mn	Fe	Co	Ni	Cu	Mo	W
Alloy 625	0.01	0.26	0.09	0.007	0.001	0.26	21.94	0.06	0.46	0.1	60.14	–	9.06	–
Stellite 6	1.2	–	0.1	0.01	<0.01	–	30.7	0.5	2	58.1	2.7	–	0.5	4.2
W–Cu–Ni	–	–	–	–	–	–	–	–	–	–	<5	<5	–	95
W	–	–	–	–	–	–	–	–	–	–	–	–	–	99.95
SiC	30	–	70	–	–	–	–	–	–	–	–	–	–	–

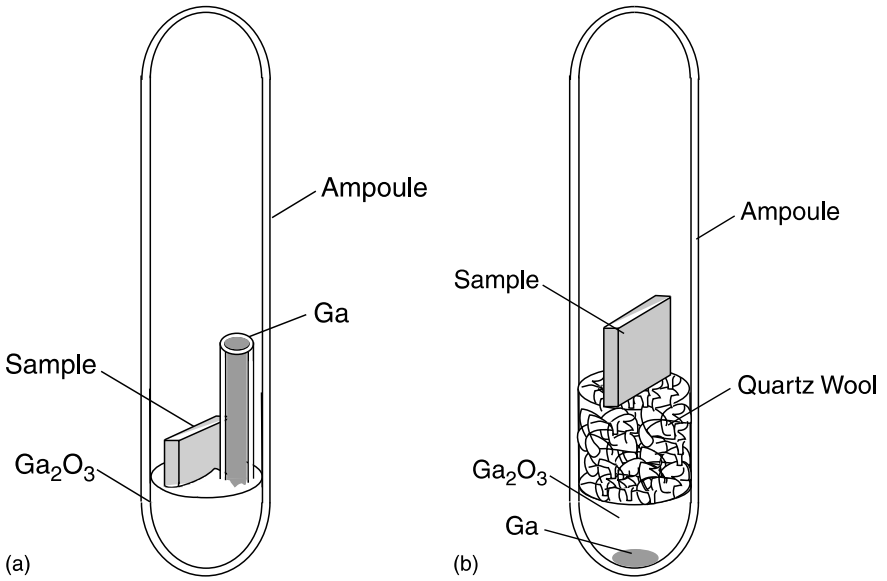

Fig. 1. Schematics are shown for ampoule configurations in which (a) the sample is in contact with Ga_2O_3 powder and (b) the sample is isolated by a plug of fused silica.

determine times at which measurable effects occurred for several of the materials. After an experiment, the ampoule was removed from the furnace and air cooled to room temperature. At this point, the ampoule was opened and the sample was weighed and placed in an evacuated storage container with desiccant until further analysis could be conducted. Exposed samples were examined using optical microscopy, scanning-electron microscopy (SEM), energy-dispersive spectroscopy (EDS), X-ray diffraction (XRD), and X-ray photoelectron spectroscopy (XPS). The surfaces prepared by polishing were directly examined after exposure, and cross-sections of the exposed samples were then cut, polished, and also examined.

3. Results

3.1. Mass changes and visual observations

A comparison of sample mass prior to and following exposure to the Ga_2O-rich atmosphere in an ampoule at 1000 °C provides a measure of reactivity for a given material. A mass gain is expected when reaction products are deposited on the sample, while a mass loss would indicate removal of material through gaseous transport or the flaking off of corrosion products. Because different samples typically had different original shapes, with different ratios of surface area to volume, comparisons of mass change between samples has limited quantitative meaning. However, mass changes offer a useful qualitative comparison of performance. The mass changes of samples after exposure to Ga_2O in sealed ampoules at 1000 °C are given in Table 2. Experiments of 2 h duration used the ampoule configuration shown in Fig. 1(a), for which the sample was in direct contact with Ga_2O_3 powder. Differentiation between corrosion products and Ga_2O_3 powder left on the sample surface after exposure was difficult. For this

Table 2
Mass changes are given after exposure to Ga_2O at 1000 °C

Material	Ampoule type	Time (h)	Mass (g)		Change (%)
			Initial	Final	
Alloy 625	a	2	4.0724	4.0840	0.3
	b	20	3.6430	4.0340	11.0
Stellite 6	a	2	2.2645	2.3940	5.7
	b	20	5.8495	6.2272	6.5
W–Cu–Ni	a	2	9.3420	9.3970	0.6
	a	2	9.7150	9.7540	0.4
	b	20	7.5051	7.9632	6.1
	b	20	6.8290	7.3734	8.0
	b	20	6.1701	6.4083	3.9
W	b	20	0.2220	0.2224	<0.2
	b	20	0.3630	0.3632	<0.2
	b	20	0.3412	0.3415	<0.2
SiC	b	20	0.4140	0.4141	<0.2
	b	20	0.3265	0.3270	<0.2

Ampoule type a: Sample in contact with Ga_2O_3 powder; Ampoule type b: Sample separated from Ga_2O_3 powder.

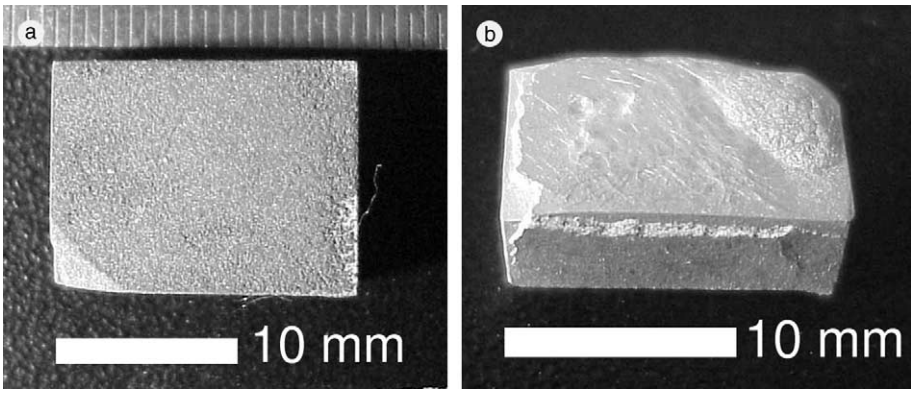

Fig. 2. Photographs of samples exposed to Ga_2O at 1000 °C for 20 h are shown for (a) Stellite 6 and (b) the W–Cu–Ni alloy.

reason, the ampoule configuration shown in Fig. 1(b) was used for all experiments of 20 h duration.

Alloy 625 shows increases in mass of 0.3% after 2 h and 11% after 20 h of exposure at 1000 °C. This material produced, after 20 h, the highest change in mass of all materials studied and appears to readily react with Ga_2O at 1000 °C. A comparison of as-received and exposed surfaces shows a significant buildup of reaction products after exposure for 20 h. This layer of silver-grey corrosion products has a rough, uneven appearance in comparison with the original polished surface. Stellite 6 exhibits a similar corrosion layer after exposure for 20 h, but the corrosion products detach from the sample as flakes more easily. A sample of Stellite 6 exposed for 20 h at 1000 °C is shown in Fig. 2(a). The Stellite 6 has an anomalously high weight gain of 5.7% after 2 h of exposure in contact with Ga_2O_3 powder, but exhibits a more reasonable weight gain of 6.5% after exposure for 20 h when separated from Ga_2O_3 powders. The unexpected large weight gain of Stellite 6 after 2 h of exposure may be the result and Ga_2O_3 powder attached to the sample surface.

The W–Cu–Ni alloy exhibits a mass increase of up to 0.6% after 2 h and an average increase of 6.0% after 20 h of exposure. Despite showing less weight gain after 20 h than the Alloy 625 sample, the corrosion layer produced on the W–Cu–Ni alloy appears the largest. The thickness of this corrosion layer varies significantly with location on the sample, as shown in Fig. 2(b). In some regions, the layer exceeds a millimeter in thickness. The corrosion layer is compact and difficult to remove from the bulk material. The corrosive attack of one sample of W–Cu–Ni alloy was so severe that the sample split open. In contrast to W–Cu–Ni, the high-purity W exhibited almost no attack. The average mass change of a high-purity W sample exposed for 20 h at 1000 °C was measured to be less than 0.2%. The only effect noticeable by visual inspection of high-purity W after exposure is a slight color change. SiC has results similar to those of the tungsten foil. Samples of SiC exposed for 20 h at 1000 °C exhibit less than a 0.2% change in mass. Visual inspection after exposure revealed no noticeable changes in the SiC material.

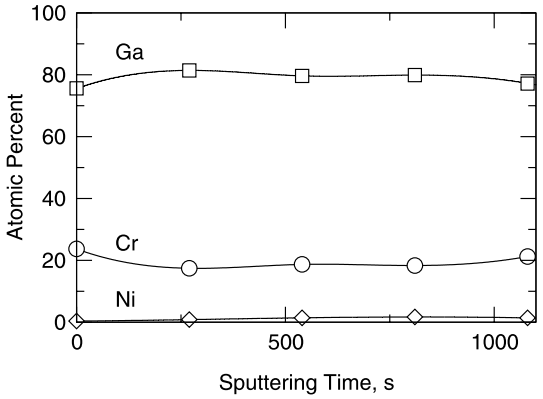

Fig. 3. XPS data for Cr, Ni, and Ga concentrations are shown as at. pct. versus sputtering time for Alloy 625 after exposure to Ga_2O for 2 h at 1000 °C.

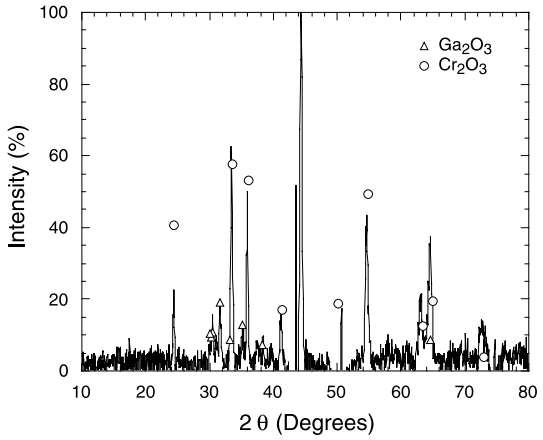

Fig. 4. XRD data are shown for Alloy 625 after exposure to Ga_2O for 2 h at 1000 °C.

3.2. Alloy 625

XPS data taken from the surface of an Alloy 625 sample exposed to Ga_2O in the first ampoule configuration, Fig. 1(a), for 2 h at 1000 °C are presented in Fig. 3 as at. pct. versus sputtering time. All XPS data were acquired using a sputtering current of 1 μA; sputtering times have not been correlated with depth for the materials studied. The elements Ga and Cr are most abundant in the sample surface, and the concentrations of these vary inversely to each other. Ni concentration in the sample surface is negligible. XRD confirms the presence of both Ga_2O_3 and Cr_2O_3 in the sample surface, as indicated by the data presented in Fig. 4. Cr_2O_3 exhibits stronger peaks than Ga_2O_3 for this sample. A sample of Alloy 625 was sectioned for SEM and EDS evaluation after exposure for 20 h at 1000 °C in an ampoule with the configuration shown in Fig. 1(b). An SEM image from the cross-section of this sample is shown in Fig. 5, with the sample surface at the right of the image. A layer of scale is clearly visible at the sample

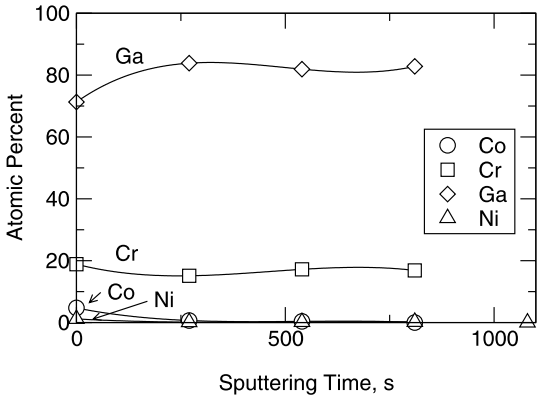

Fig. 6. XPS data for Co, Cr, Ni, and Ga concentrations are shown as at.% versus sputtering time for Stellite 6 after exposure to Ga_2O for 2 h at 1000 °C.

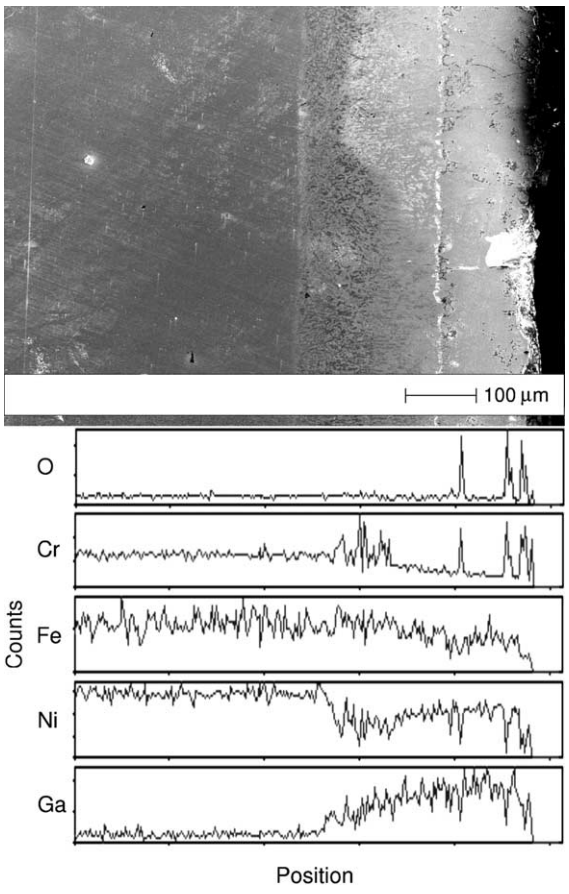

Fig. 5. An SEM image of a cross-section of Alloy 625 exposed to Ga_2O for 20 h at 1000 °C is shown with EDS line-scan data for the elements O, Cr, Fe, Ni, and Ga.

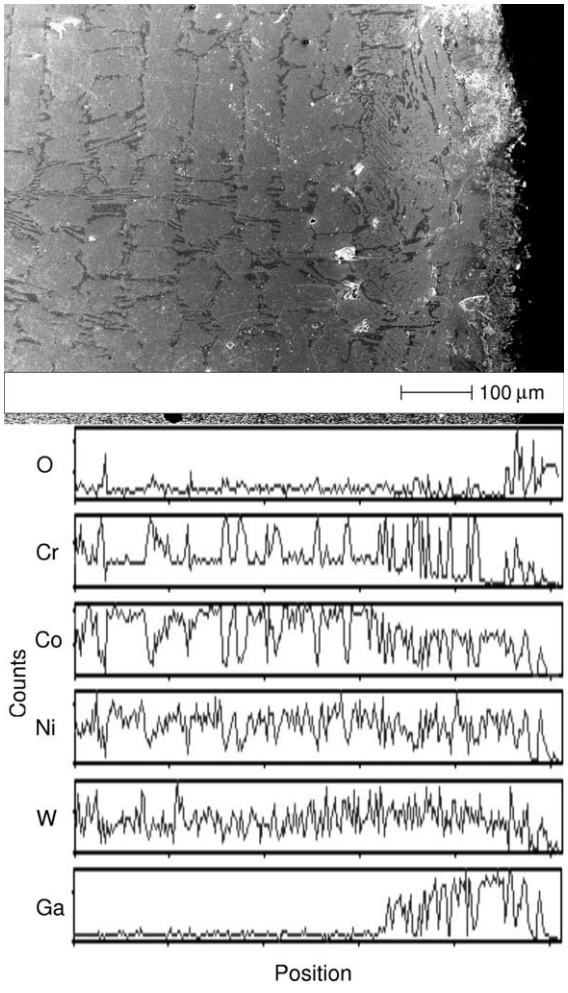

Fig. 7. An SEM image of a cross-section of Stellite 6 exposed to Ga_2O for 20 h at 1000 °C is shown with EDS line-scan data for the elements O, Cr, Co, Ni, W, and Ga.

surface, and a reaction zone is evident in the sample below this layer. This altered microstructure gives way to a microstructure characteristic of the base material as depth increases toward the left of the image.

EDS line-scan data are included below the SEM image in Fig. 5; data are presented as normalized counts for each element versus position corresponding to the SEM image. EDS data for O, Cr, Fe, Ni, and Ga are presented. The EDS data of Fig. 5 indicate that O concentration closely tracks Cr concentration, both of which are elevated in the sample surface. Peaks in Cr and O concentration are evident at the outer surface of the scale layer and at the interface of the scale and sample. Cr concentration also increases at the base of the reaction zone. Ga concentration is highest in the scale at the sample surface and decreases through the reaction zone. The limit of Ga diffusion into the base material corresponds with the depth of the reaction zone. Ni concentration is lower in the reaction zone and scale than in the base material. The concentration of Ga varies in an inverse fashion to the concentration of Cr.

3.3. Stellite 6

XPS data taken from the surface of a Stellite 6 sample exposed to Ga_2O for 2 h at 1000 °C are presented in Fig. 6 as at. pct. versus sputtering time. Both Co and Ni have negligible concentrations in the sample surface. Ga and Cr are the most abundant elements in the surface of the sample, and their concentrations exhibit approximately the same inverse dependence observed in the surface of the exposed Alloy 625 sample. XRD data from Stellite 6 exposed to Ga_2O indicate the presence of Cr_2O_3 and some Ga_2O_3 in the sample surface, as also seen for Alloy 625.

A sample of Stellite 6 was sectioned for SEM and EDS evaluation after exposure to Ga_2O for 20 h at 1000 °C in the second ampoule configuration. An SEM image from this cross-sectioned sample is shown in Fig. 7. The base Stellite 6 material, in the left portion of the image, exhibits the same two-phase microstructure characteristic of the as-received material. One phase is Co-rich and the other Cr-rich, as can be seen from the EDS line scans for Co and Cr, shown at the bottom of Fig. 7. The surface of the Stellite 6 sample in Fig. 7 exhibits a thin oxide scale, as evident from the EDS line scan for O, shown directly below the SEM image. EDS line-scan data for Cr and O suggest that this scale is composed primarily of Cr_2O_3. Below the oxide scale, a reaction zone containing Ga is evident. The penetration of Ga indicates that Stellite 6 is highly susceptible to Ga attack under the experimental conditions. Fig. 8 contains EDS data from this same sample, but in the form of element maps. Fig. 8(a) contains an SEM image of the area from which data for the element maps were obtained. Fig. 8(b)–(d) contain element maps for Co, Cr, and Ga, re-

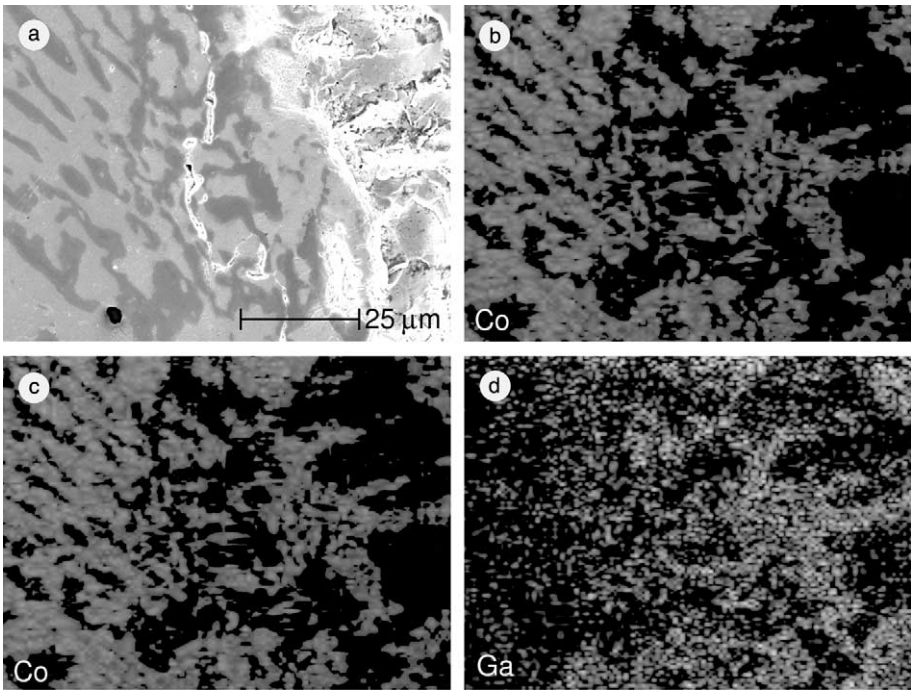

Fig. 8. EDS element maps of a cross-section of Stellite 6 exposed to Ga_2O for 20 h at 1000 °C are shown for the elements (b) Co, (c) Cr, and (d) Ga along with (a) an SEM micrograph of the same region.

spectively. Regions of high Ga concentration clearly follow the regions of high Co concentration, which correspond to the Co-rich phase in Stellite 6. This selection of the Co-rich phase as the preferred diffusion path for Ga penetration into Stellite 6 is consistent with the high diffusivity and solubility of Ga in Co observed by Kolman et al. [8].

3.4. W–Cu–Ni alloy

A sample of the W–Cu–Ni alloy was sectioned for SEM and EDS examination after exposure for 20 h at 1000 °C in the second ampoule configuration. An SEM image of this sectioned sample is shown in Fig. 9. The W–Cu–Ni alloy exhibits a relatively discrete reaction zone at its surface, while the material to the left of the reaction zone is characteristic of the as-received material. EDS line-scan data are shown directly below the SEM image in Fig. 9. The reaction zone is composed primarily of Ni, Cu and Ga. No significant concentrations of W are detected in the reaction zone. O content in the reaction zone is no higher than in the base material, indicating that this reaction zone is most likely not an oxide scale. Fig. 10 contains EDS data in the form of element maps from the same sample shown in Fig. 9. Fig. 10(a) is an SEM image of the area from which element maps are constructed. Fig. 10(b)–(e) are element maps for W, Ni, Cu, and Ga, respectively. The base material contains two phases, one which contains primarily W and a second which is composed of a Cu–Ni solid solution. These phases are clearly distinguishable in the element maps of Fig. 10. The element maps show a reaction zone at the sample surface which is rich in Ni, Cu, and Ga. Ga is seen to penetrate deeply beyond the reaction zone at the surface by means of the Cu–Ni phase. This result is consistent with the penetration of Ga into Cu interphase regions observed by Kolman et al. in a W–Cu alloy [8]. The W phase shows little to no reaction with or absorption of Ga. Cu and Ni appear to have diffused from the base metal to interact with Ga in creating the reaction zone at the sample surface.

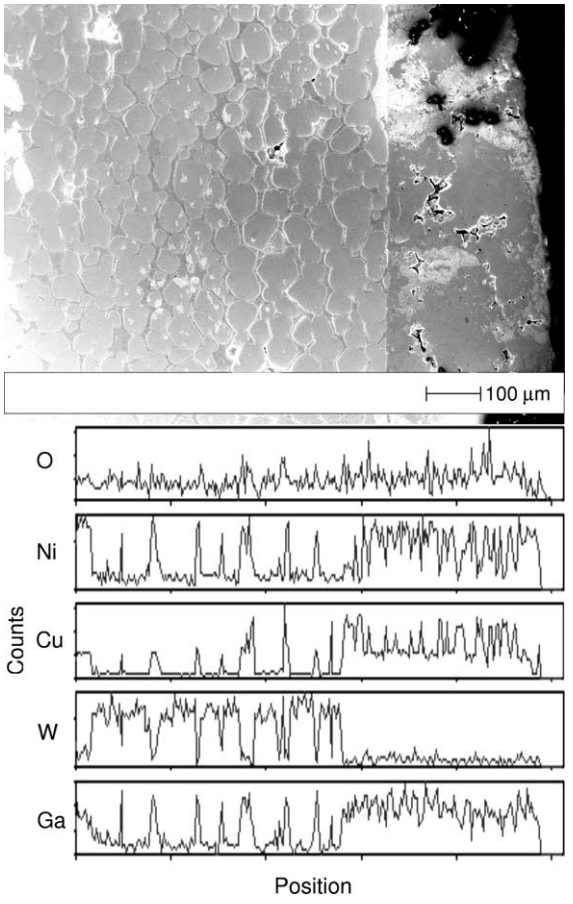

Fig. 9. An SEM image of a cross-section of the W–Cu–Ni alloy exposed to Ga_2O for 20 h at 1000 °C is shown with EDS line-scan data for the elements O, Ni, Cu, W, and Ga.

3.5. High-purity W

A sample of the high-purity W material was sectioned for SEM and EDS examination after exposure to Ga_2O for 20 h at 1000 °C in the second ampoule configuration. An SEM image of this sample is shown in Fig. 11 along with EDS line-scan data for the elements O, W, and Ga. Neither significant scale nor a reaction zone are observable at the surface of the sample. The EDS line-scan for O shows an increase in O concentration just at the sample's surface, which might indicate a very thin (< 1 μm) oxide layer. The Ga concentration shown by EDS is uniformly small, indicating concentrations no higher than might be expected from slight contamination by surface residue during metallographic preparation of the sectioned sample.

3.6. Silicon carbide

A sample of SiC was sectioned for SEM and EDS examination after exposure to Ga_2O for 20 h at 1000 °C in the second ampoule configuration. An SEM image of this sample is shown in Fig. 12 along with EDS line-scan data for the elements C, O, Si, and Ga. Neither a scale nor a reaction zone are observed at the surface of the sample. The EDS line-scan data for O indicate an elevated O content in a very thin region (<1 μm) at the sample surface. This is interpreted as a thin layer of SiO_2, which is commonly expected to form on the surface of SiC at elevated temperatures when O_2 is present. The high C content shown to the right of the sample in the EDS line-scan data is an artifact from the carbon

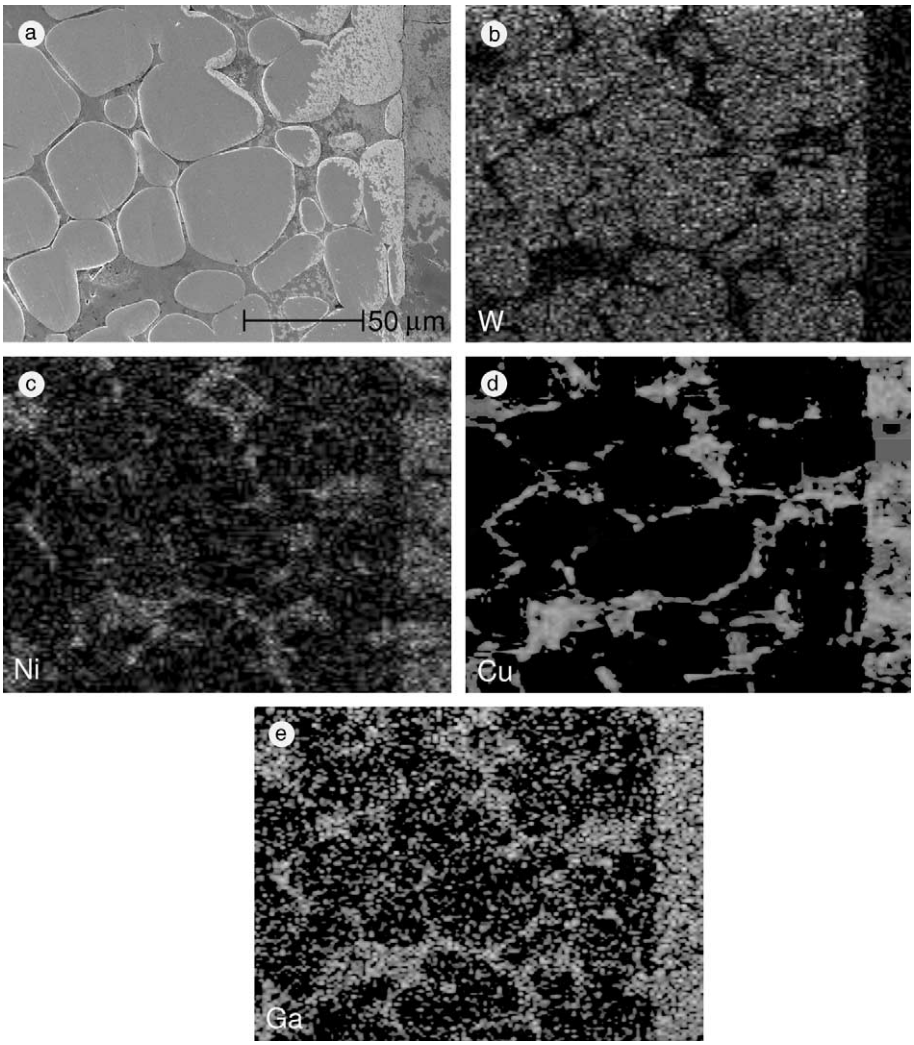

Fig. 10. EDS element maps of a cross-section of the W–Cu–Ni alloy exposed to Ga_2O for 20 h at 1000 °C are shown for the elements (b) W, (c) Ni, (d) Cu, and (e) Ga along with (a) an SEM micrograph.

tape used in mounting the sample for SEM observation. A uniform low Ga concentration is seen in the EDS line-scan data. The concentration of Ga is no higher than might be expected from slight contamination during metallographic preparation of the sectioned sample.

4. Conclusions

Among the five materials tested, Alloy 625 and Stellite 6 show the highest susceptibilities to corrosive attack under the experimental conditions studied. The poor performance of Alloy 625 at 1000 °C is consistent with its poor resistance to Ga at lower temperatures [9]. The poor performance of Stellite 6 is likely associated with both the high solubility of Ga in Co [10], which is a primary component of this alloy, and with its high Cr content. Cr appears to play a significant role in corrosive attack of both these alloys by Ga_2O. A possible mechanism for this is oxidation of Cr by Ga_2O, see Ref. [10],

$$2\,Cr(s) + 3\,Ga_2O(g) \rightarrow Cr_2O_3(s) + 6\,Ga(l), \quad (4)$$

producing liquid Ga at the sample surface, which may then penetrate the sample by diffusion. The W–Cu–Ni alloy was attacked aggressively at the Cu–Ni phase regions, but the high-purity W shows a high resistance to corrosive attack by Ga_2O. The attack of the Cu–Ni phase regions is consistent with the poor resistance of both Cu and Ni to Ga [10]. The SiC material is resistant to corrosive attack by Ga_2O and exhibits no significant

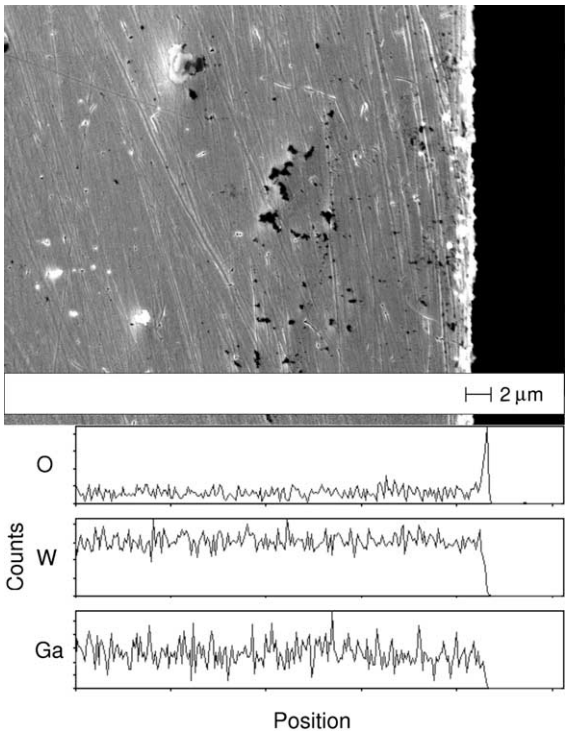

Fig. 11. An SEM image of a cross-section of high-purity W exposed to Ga_2O for 20 h at 1000 °C is shown with EDS line-scan data for the elements O, W, and Ga.

corrosion products. High-purity W and SiC have the greatest potential for constructing durable furnace parts which will be exposed to Ga_2O.

Acknowledgements

This work was supported under the auspices of Los Alamos National Laboratory and the Amarillo National Resource Center through project number 746BH-001802G.

References

[1] T.M. Besmann, J. Am. Ceram. Soc. 81 (1998) 3071.
[2] D.F. Wilson, E.C. Beahm, T.M. Besmann, J.H. DeVan, J.R. DiStefano, U. Gat, S.R. Greene, P.L. Rittenhouse, B.A. Worley, Potential Effects of Gallium on Cladding Materials, Oak Ridge National Laboratory, Oak Ridge, TN, Technical Report No. ORNL/TM-13504, October 1997, p. 20.

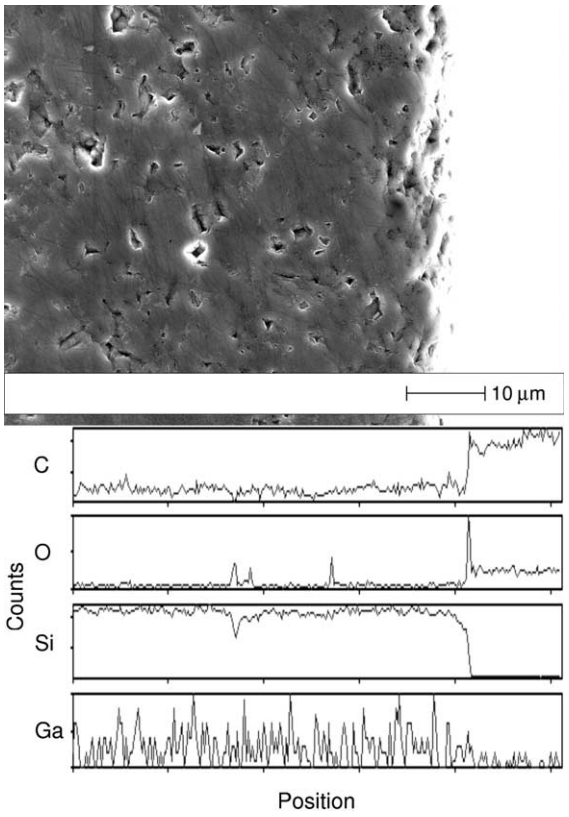

Fig. 12. An SEM image of a cross-section of SiC exposed to Ga_2O for 20 h at 1000 °C is shown with EDS line-scan data for the elements C, O, Si, and Ga.

[3] D.P. Butt, Y. Park, T.N. Taylor, J. Nucl. Mater. 264 (1999) 71.
[4] C.V. Philip, W.W. Pitt, C. Beard, Investigations in Gallium Removal, Amarillo National Research Center for Plutonium, Amarillo: Amarillo, TX, 1997, Report no. ANRCP-1997-3, p. 6.
[5] D.G. Kolman, M.E. Griego, C.A. James, D.P. Butt, J. Nucl. Mater. 282 (2000) 245.
[6] D.G. Kolman, Corros. Sci. 43 (2001) 99.
[7] M.G. Fontana, in: Corros. Eng., 3rd Ed., McGraw-Hill, New York, 1986, p. 410.
[8] D.G. Kolman, T.N. Taylor, Y.S. Park, M. Stan, D.P. Butt, C.J. Maggiore, J.R. Tesmer, G.J. Havrilla, Oxid. Met. 55 (2001) 437.
[9] P.R. Luebbers, O.K. Chopra, Proceedings of the 1995 16th IEEE/NPSS Symposium on Fusion Engineering, Part 1 (of 2), p. 232, October 1–5, 1995, Champaign, IL, USA.
[10] D.G. Kolman, T.N. Taylor, Y.S. Park, M. Stan, D.P. Butt, C.J. Maggiore, J.R. Tesmer, G.J. Havrilla, Oxid. Met. 56 (2001) 347.
[11] I.A. Sheka, I.S. Chaus, T.T. Mityureva, in: The Chemistry of Gallium, Elsevier, New York, 1966, p. 10.